Synthesis of $MgAl_2O_4$ spinel nanoparticles via polymer-gel and isolation-medium-assisted calcination

Xuelian Du,[a] Yaqiang Liu, Liqiang Li, and Wencong Chen
Physics Department, Shangqiu Normal University, Shangqiu 476000, China
Yuting Cui[b]
Physics Department, Chongqing Normal University, Chongqing 404100, China

(Received 1 July 2014; accepted 8 October 2014)

Magnesium aluminate ($MgAl_2O_4$) spinel nanoparticles with an average crystalline size of 35 nm were synthesized by polymer-gel and isolation-medium-assisted calcination. In the process, a large excess of MgO, 40 times the stoichiometric amount of spinel, is added to the precursor mixture to separate the spinel particles as they are nucleated to prevent their agglomeration and coarsening during calcination. Well-dispersed $MgAl_2O_4$ nanoparticles with a single-crystal structure were obtained after acid washing of calcined product. The microstructures of the as-prepared samples were characterized by differential thermal and thermogravimetric analysis, x-ray diffractometry, Fourier transform infrared spectroscopy, nitrogen adsorption–desorption isotherms, scanning electron microscopy, energy-dispersive x-ray spectroscopy, and transmission electron microscopy. The results indicate that MgO acting as the isolation medium is effective in preventing the agglomeration of $MgAl_2O_4$ nanoparticles, and it also prevents their contamination by introducing an isolation medium during the preparation process. The nanopowder was sintered up to 95% of the theoretical density but with parallel grain growth.

I. INTRODUCTION

Magnesium aluminum ($MgAl_2O_4$) spinel is considered to be an important ceramic material, and it possesses attractive features such as high mechanical strength, good chemical stability, high thermal shock resistance, and low electrical losses.[1–3] It also has apparent optical properties, which are similar to those of glass, and it has been applied in lighting and laser technologies.[4–6] $MgAl_2O_4$ spinel ceramic is one of the main materials used in military and space applications because of its simple synthesis, excellent mechanical properties, and transparency over a wide range of 0.2–6 μm.[7–9] The potential applications of $MgAl_2O_4$ spinel ceramic materials are therefore vast. Ceramic powder preparation is fundamental in the synthesis and application of ceramic materials. $MgAl_2O_4$ nanoparticles with a narrow size distribution and a low degree of agglomeration are desirable in these applications.

Various approaches have been used to synthesize disperse $MgAl_2O_4$ spinel nanoparticles, such as solid-state reaction, co-precipitation, and sol–gel syntheses.[10–13] Among these, the solid-state reaction route is suitable for producing nanoparticles on a large-scale, but it usually results in particle coarsening because of high reaction temperature used. The co-precipitation route is simple, economical, and suitable for industrial production, but the as-prepared particles are agglomerated sometimes. Ultrafine particles can be obtained by the sol–gel route, but partial sintering occurs. The sintering, coarsening, and hard agglomeration of particles are unfavorable for their performance and application, especially in ceramic green body densification during sintering.[14,15] The simple synthesis of well-dispersed $MgAl_2O_4$ spinel nanoparticles therefore still poses a challenge.

In this paper, we report a simple method to synthesize well-dispersed $MgAl_2O_4$ spinel nanoparticles. The method is based on the concept of isolation-medium-assisted calcination.[16] In the process, excess magnesium salt than its stoichiometry is introduced during precursor preparation, and a large excess of MgO is formed in the precursor mixture during calcination. A small amount of MgO acts as the reactant to synthesize target product via a solid-state reaction, while most of MgO acts as the isolation medium to separate the spinel particles as they are nucleated and to prevent their agglomeration and coarsening during calcination. The results indicate that using MgO as the isolation medium to assist calcination can prevent the agglomeration and contamination of $MgAl_2O_4$ nanoparticles. This study uses a modified sol–gel method to synthesize well-dispersed $MgAl_2O_4$ spinel nanoparticles. The changes in crystalline structure, crystallite size, specific surface area, and particle morphology were studied.

Address all correspondence to these authors.
[a]e-mail: xueliandu@126.com
[b]e-mail: cytcyt111@163.com
DOI: 10.1557/jmr.2014.341

II. EXPERIMENTAL PROCEDURE

A. Sample preparation

A solution was prepared from aluminum nitrate ($Al(NO_3)_3 \bullet 9H_2O$) and magnesium nitrate ($Mg(NO_3)_2 \bullet 6H_2O$) dissolved in deionized water. The concentration of Al^{3+} ions was adjusted to 0.005 M and the Mg/Al atomic ratio was 20. Acrylamide (C_3H_5NO) and *N*,*N*′-methylenebisacrylamide ($C_7H_{11}N_2O_2$) were used as the polymer monomer and crosslinker, respectively, and added to the solution. The molar ratios of polymer monomer to Al^{3+} ions and monomer to crosslinker were adjusted to 40 and 25, respectively. The mixture was stirred at room temperature until the polymer network agent dissolved. Ammonium persulfate [$(NH_4)_2S_2O_8$] used as the initiator was introduced into the solution to promote the polymerization reaction of a network agent. The molar ratio of the polymer monomer to the initiator was adjusted to 20. The solution was stirred until an ivory polymer gel was formed. The precursor, a metal ion polymer complex, was obtained after drying the polymer gel at 80 °C. The precursors were calcined at 500–1000 °C, and the calcined products were washed once with 3 M dilute hydrochloric acid and twice with deionized water to obtain the samples. All the chemical reagents were purchased from Sinopharm Chemical Reagent Co., Ltd, China.

B. Characterization

The thermal behavior of the precursor was examined by thermogravimetric-differential thermal analysis (TG-DTA) on a Netzsch STA 449C thermal analyzer (Wald-kraiburg, Germany) at a heating rate of 10 °C/min. Crystal structures of the samples were analyzed by x-ray diffraction (XRD) on a Rigaku D/max-2400 diffractometer (Tokyo, Japan) using nickel filtered Cu K_α radiation in the 2θ range of 10°–80°. Crystallinity degree of the sample was estimated quantitatively from the relative areas of crystalline and amorphous regions from the diffraction pattern after drawing a smooth curve with the help of MDI Jade 5 x-ray data analysis program.[17] The average crystal size (D_{XRD}) of $MgAl_2O_4$ nanoparticles was calculated using the Scherrer formula: $D_{XRD} = \frac{0.89\lambda}{\beta \cos\theta}$, where λ is the radiation wave length (0.15406 nm), β is the full width at half maximum of the diffraction peaks, and θ is the Bragg angle. The specific surface areas of the samples were determined by N_2 adsorption–desorption isotherms using an ASAP 2010 Micrometrics, and the equivalent average particle size (D_{BET}) was calculated via the formula: $D_{BET} = {}^{6}/_{(\rho S_w)}$, where $\rho = 3.55$ g/cm^3 is the theoretical density for $MgAl_2O_4$ spinel and S_w is the specific surface area of the sample. The infrared spectra of the samples were measured by a Nicolet NEXUS 670 Fourier transform infrared spectrometer (FTIR; Thermo Scientific, Waltham, MA) in the range of 400–4000 cm^{-1} to identify the nature of bonding in the samples. The microstructures of the samples and the sinter were analyzed by a scanning electron microscope (SEM, Hitachi S-4800, Japan) and a transmission electron microscope (TEM, Tecnai G^2 F30, Hillsboro, OR). The particle size distribution was calculated from the TEM micrograph using Gatan Digital Micrograph analysis software. The relative density of the sintered spinel pellet was evaluated using the Archimedes method.

III. RESULTS AND DISCUSSIONS

The TG-DTA curves for the as-prepared precursor are shown in Fig. 1. The DTA curve shows one endothermic and three exothermic events, and the corresponding TG curve shows three mass losses. A broad endothermic peak ranging from 60 to 240 °C is accompanied by a mass loss of 16.1%, and is attributed to the removal of free water and hydrate water.[18] The sharp exothermic peak at 275 °C, accompanied by a mass loss of 19.4%, is attributed to the oxidation of residual nitrate ions in the precursor.[19] It is well known that the degradation of polyacrylamide network is a multistep process and is completed at 300–600 °C under the air atmosphere.[18,20,21] The broad exothermic peaks centered at 376 °C, accompanied by a mass loss of 29%, are assigned to a major decomposition of polymer.[18,20,21] The strong exothermic peak at 608 °C, accompanied by a mass loss of 18.6%, can be attributed to the thermal overlap of the crystallization transition, in which the amorphous oxide becomes nanocrystallite and the lattice energy is released, and burning and oxidation of residual polymer.[21,22] A weak endothermic peak at 650–800 °C with no obvious mass losses is due to the solid-state reaction of Al_2O_3 to MgO and the formation of $MgAl_2O_4$ grains.[21] The weak

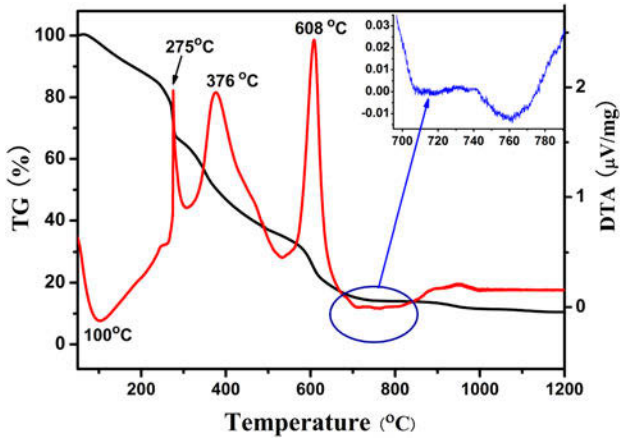

FIG. 1. TG-DTA curves of the as-prepared spinel precursor.

exothermic effect occurs above 800 °C, accompanied by a slight weight loss of 2.3%, is associated with the final spinel crystallization step and the oxidation of the residue carbon.[18,23]

Figure 2 shows XRD spectra of the samples obtained by calcining the precursors at different temperatures for 2 h before [Fig. 2(a)] and after [Fig. 2(b)] washing with dilute hydrochloric acid and water. The XRD spectra of calcined products at 500–900 °C [Fig. 2(a)] display sharp and strong diffraction peaks mostly due to cubic MgO species (space group *Fm*−3*m*, JCPDS No. 43-1022). Due to a gradual degradation of the metal ion polymer complex, some diffraction peaks related to the magnesium sulfate complex are observed at 500–800 °C. After calcination at 900 °C, both cubic MgO and $MgAl_2O_4$ spinel are detected. From Fig. 2(a), it can be seen that a large amount of cubic MgO in the calcined product is present. After washing with dilute hydrochloric acid and water, XRD spectra of the samples are shown in Fig. 2(b). The diffuse peaks of the sample prepared at 500 °C indicate the formation of an amorphous phase. The major diffraction peaks of $MgAl_2O_4$ spinel at $2\theta = 31.27°$ for (220), 36.85° for (311), 44.83° for (400), 59.37° for (511), and 65.24° for (440) appear in the XRD spectrum of the sample prepared at 700 °C. This indicated that $MgAl_2O_4$ spinel was formed after 700 °C calcination, and it is consistent with the DTA result (the endothermic peak at 650–800 °C in Fig. 1). These $MgAl_2O_4$ diffraction peaks gradually become stronger with increasing calcination temperature up to 800 °C. After calcination at 900 °C, the diffraction spectrum of the sample shows the characteristic diffraction peaks of cubic $MgAl_2O_4$ (JCPDS No. 21-1152). No residual MgO impurity is detected, although this compound is observed in other methods.[24]

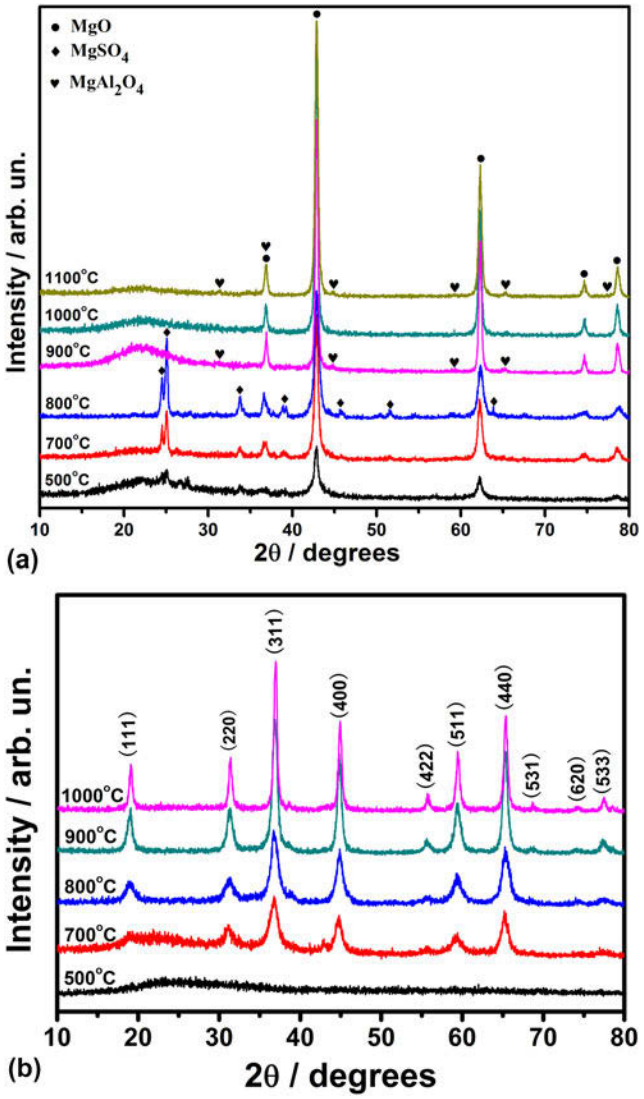

FIG. 2. XRD spectra of the calcined products at different temperatures for 2 h, before [Fig. 2(a)] and after [Fig. 2(b)] washing with dilute hydrochloric acid and deionized water.

The degree of crystallinity, specific surface area, and crystalline size of the sample obtained at different temperatures are shown in Table I. The degree of crystallinity and the crystalline size increase with increasing calcination temperatures from 700 to 1000 °C. After calcining at 900 °C, an almost pure $MgAl_2O_4$ spinel phase is obtained. The crystalline size of the spinel sample increases slowly with increasing calcination temperatures from 900 to 1000 °C, and it can be confirmed by the XRD pattern [Fig. 2(b)], in which there is no obvious sharpening of diffraction peaks with the increase in calcination temperature. This can be attributed to the isolation effect of isolating medium.

FTIR spectra of the precursor and the samples obtained at different temperatures are shown in Fig. 3. In all curves, the absorption bands at ≈3450 and 1630 cm^{-1} are observed. These are related to O–H stretching vibration and H_2O deformation vibration, respectively, and can be attributed to the presence of a hydroxyl group in polymeric gel and adsorption water from air by nanosized samples with high surface area.[25] With an increase in

TABLE I. Degree of crystallinity, specific surface area, and crystalline size (D_{XRD} and D_{BET}) of spinel samples obtained at different temperatures.

Calcination temperature (°C)	Crystallinity (%)	Crystalline size (nm) D_{XRD}	Specific surface area (m^2/g)	Crystalline size (nm) D_{BET}
500	...	...	254.3	n.d.
700	4.72	12.6	179.7	9.4
800	23.76	14.1	133.4	12.7
900	95.63	25.7	64.8	26.5
1000	99.7	30.5	52.9	31.9

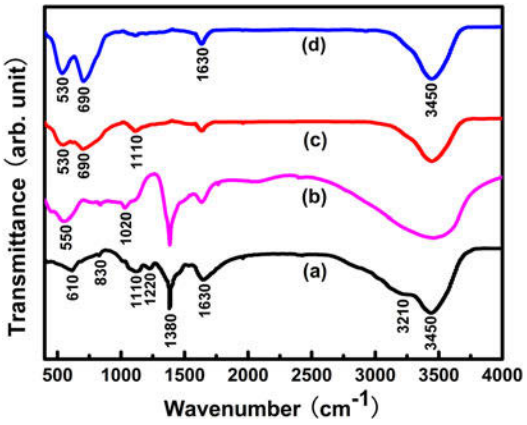

FIG. 3. FTIR spectra of the polymeric gel precursor (a) and spinel samples obtained at different temperatures: 500 °C (b), 700 °C (c), and 1000 °C (d).

calcination temperature, the intensities of these absorption bands gradually weakened. This is simply attributed to the decrease in the surface area of the powder. The presence of NO_3^- is evidenced by the absorption bands at 1380 and 830 cm^{-1} (Ref. 26). The bands disappear with an increase in calcination temperature up to 700 °C, because of a complete oxidation of nitrate ions. The absorption bands at 1000–1300 cm^{-1} are consistent with stretching vibrations of C–O–C polymer groups.[20] These bands disappear gradually with an increase in calcination temperature. Below 1000 cm^{-1}, the absorption bands are related to the Al–O inorganic network. For the six-coordinated AlO_6 groups, Al–O stretching and bending vibrations are expected at 500–700 and 330–450 cm^{-1} (Ref. 27). For the four-coordinated AlO_4 groups, Al–O stretching and bending modes are expected at 700–850 and 250–320 cm^{-1} (Ref. 27). In curves A and B of Fig. 3, the absorption bands at 3450, 550, and 600 cm^{-1} are relatively broad. This can be attributed to continuous distribution of the bond length in the amorphous structure and to various distortions in the polymer-gel precursor.[20,25,28] In curves B and C, the two strong absorption bands at 530 and 690 cm^{-1} are related to the AlO_6, inorganic network groups. These build up the spinel structure and therefore indicate the formation of $MgAl_2O_4$ spinel in calcined samples.[20,26,27,29] The FTIR spectra of the products are similar in spite of different synthesized methods.

The morphology and microstructure of as-prepared $MgAl_2O_4$ spinel at 1000 °C were investigated by SEM and TEM, respectively, as shown in Fig. 4. The low-magnification and panoramic views from SEM and TEM images [Figs. 4(a) and 4(b)] show the uniformity of synthesized products, and no hard agglomerates were visible in the TEM micrograph [Fig. 4(b)]. This indicates that no undesirable agglomeration of $MgAl_2O_4$

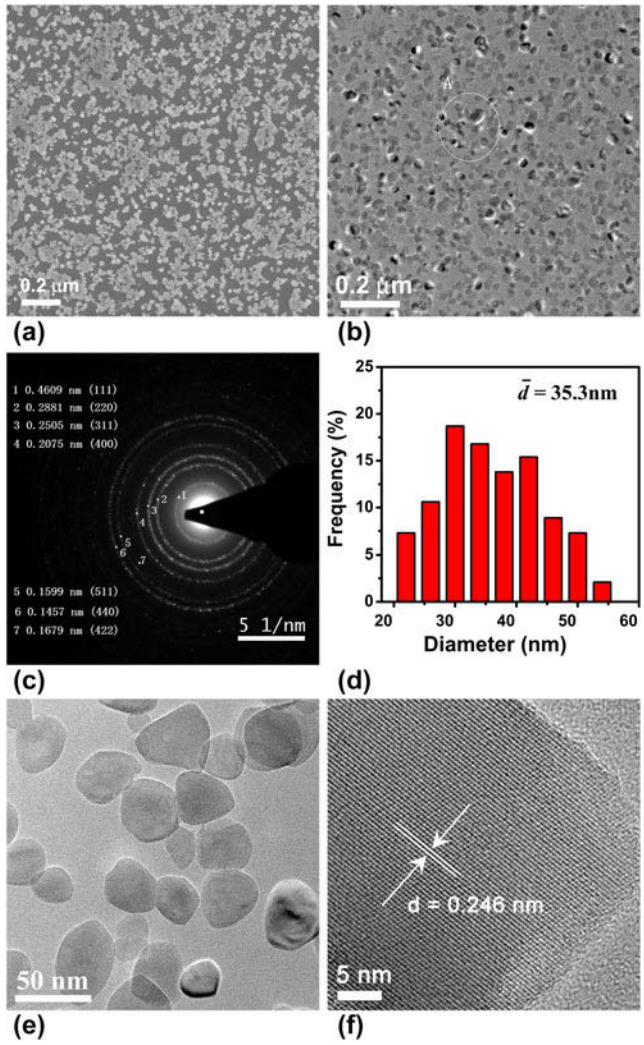

FIG. 4. Low-magnification (a) SEM and (b) TEM images for panoramic views, (c) SAED pattern, (d) particle size distribution, (e) high-magnification TEM image, and (f) HRTEM image of as-prepared $MgAl_2O_4$ nanoparticles at 1000 °C.

nanoparticles occurred during the preparation process. The selected area electron diffraction (SAED) pattern of a selected area (A) in Fig. 4(b) is shown in Fig. 4(c), and it exhibits six clear and one obscure diffraction rings with d-spacings about 0.4609, 0.2881, 0.2505, 0.2075, 0.1599, 0.1457, and 0.1679 nm, which could be attributed to (111), (220), (311), (400), (511), (440), and (422) reflections of cubic $MgAl_2O_4$ spinel structure, respectively. The particle size distribution of $MgAl_2O_4$ nanoparticles [in Fig. 4(b)] is shown in Fig. 4(d). The histograms for particle size distribution and mean particle sizes in Fig. 4(d) were determined from 280 samplings of spinel particles in the sample, using Digital Micrograph version 3.4.3 distributed by Gatan.[30] The average particle size is ≈35 nm, which is similar to the results as calculated from XRD and BET data. The magnified TEM image

in Fig. 4(e) shows that the as-prepared $MgAl_2O_4$ nanoparticles have a polyhedral morphology and are 22–52 nm in diameter. The corresponding high-resolution TEM (HRTEM) micrograph is shown in Fig. 4(f). The spacing between two lattice planes is 0.246 nm, which can be ascribed to the (311) crystal planes of $MgAl_2O_4$ spinel. It indicates the single-crystal nature of formed $MgAl_2O_4$ nanoparticles. From Fig. 4, it can be seen that well-dispersed $MgAl_2O_4$ single-crystal nanoparticles with narrow particle size distribution are obtained. The polymer-gel and isolation-medium-assisted calcination can prevent particle contact and reduce agglomeration.

The chemical stoichiometry of the as-prepared spinel sample at 1000 °C was investigated by EDS. The result (Table II) shows that the sample consists of O, Al, and Mg. C is also present as the major component of the carbon conductive tape. The Mg/Al atomic ratio of the as-prepared sample is ≈1.23:2.46, and this result confirms the formation of a pure $MgAl_2O_4$ spinel phase.

Based on the above results, the formation mechanism of well-dispersed $MgAl_2O_4$ nanoparticles can be explained as follows. A rough schematic diagram is shown in Fig. 5 to illustrate the formation of well-dispersed $MgAl_2O_4$ nanoparticles via polymer-gel and isolation-medium-assisted calcination. As shown in Fig. 5, a three-dimensional network structure formed by additional polymer network agents is used to disperse metal ions into three-dimensional grids uniformly, and the movement of Mg^{2+} and Al^{3+} ions in the mixed system is limited because of the formation of polymeric gel. It ensures that the opportunity for contacting and congregation of particles is reduced significantly during drying and the initial calcination process. During calcining, $MgAl_2O_4$ nanoparticles are fabricated in situ by a solid-state reaction of MgO and Al_2O_3 oxides, which are formed from precursor decomposition. Due to a large excess of magnesium nitrate introduced into the precursor, a large excess of MgO is formed after initial calcination. A large excess of MgO, 40 times the stoichiometric amount of spinel, separate the spinel particles as they are nucleated to prevent their agglomeration and coarsening during calcination. After calcining, excess MgO acting as the isolation medium is removed from calcined product by acid washing; and then well-dispersed $MgAl_2O_4$ nanoparticles are obtained. It is well known that a solid-state reaction for preparing $MgAl_2O_4$ nanoparticles always causes agglomeration because of the contact and growth of ultrafine particles.[24] In this work, in the solid-state reaction system, excess MgO acts not only as a reactant but also as the isolation medium. It surrounds fresh $MgAl_2O_4$ grains and prevents the contact and growth of $MgAl_2O_4$ nanoparticles, which is caused by thermal aggregation of $MgAl_2O_4$ grains. After acid washing with 3 M dilute hydrochloric acid, a large excess of MgO is removed from the samples, and $MgAl_2O_4$ particles are independent. Furthermore, excess MgO as the isolation medium also prevents the contamination of $MgAl_2O_4$ nanocrystalline by introducing an isolation medium during the preparation process. High purity $MgAl_2O_4$ nanoparticles with narrow size distribution were therefore prepared.

The sintering property of $MgAl_2O_4$ spinel nanoparticles with an average size of 35 nm was investigated. The sample was pressed into a disk (10 mm diameter, 1–2 mm thick) at 1100 MPa, and sintered by two-step sintering (at 1410 °C for 1 h and 1350 °C for 20 h) in a box furnace in air. The microstructure of as-sintered $MgAl_2O_4$ spinel ceramic is shown in the SEM micrograph of Fig. 6. The sintered spinel ceramic has a relative density of 95.2%, as determined by the Archimedes method. Equiaxial grains with clear grain boundaries and polyhedral morphologies are visible in the SEM micrograph. The average grain size is ≈317 nm, which is much smaller than that reported in the literature.[20,31] This should be attributed to its traits such as nonagglomeration, high specific surface area, and narrow particle size distribution. The sintering schedule is the important factors in affecting the final sinter microstructure.

TABLE II. EDS analysis data of as-prepared spinel samples at 1000 °C.

Sample	Element	Weight %	Atomic %	Mg/Al atomic ratio
Nanocrystalline $MgAl_2O_4$ calcined at 1000 °C	C	11.04	16.82	1.23:2.46
	O	46.98	53.66	
	Mg	12.92	9.84	
	Al	29.06	19.67	

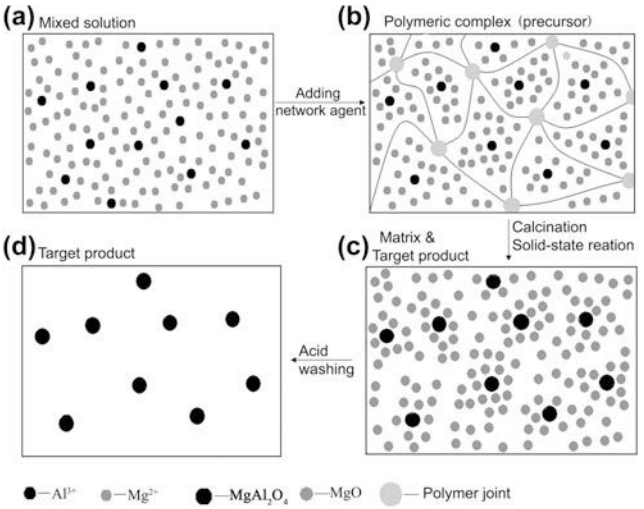

FIG. 5. A rough schematic diagram of a preparation process of well-dispersed $MgAl_2O_4$ nanoparticles.

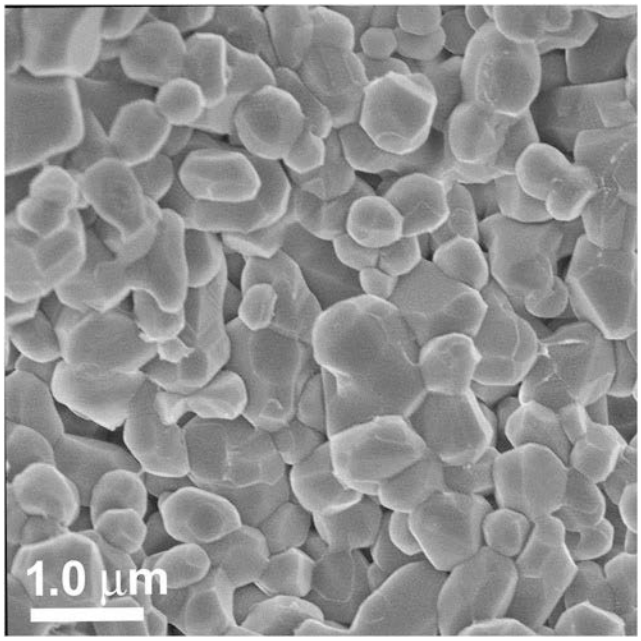

FIG. 6. SEM image of $MgAl_2O_4$ spinel ceramics from starting $MgAl_2O_4$ nanopowders with an average particle size of 35 nm, pressed at 1100 MPa, and sintered at 1410 °C for 1 h then 1350 °C for 20 h.

IV. CONCLUSION

Well-dispersed $MgAl_2O_4$ spinel nanoparticles were synthesized by a polymer-gel and isolation-medium-assisted calcination method. $MgAl_2O_4$ nanoparticles are formed in situ by a solid-state reaction of MgO and Al_2O_3 formed from decomposition of the precursor. Using excess MgO substrate in the solid-state reaction system as an isolation medium prevents the contact and growth of fresh $MgAl_2O_4$ nanoparticles and ensures the production of a product of high purity. TEM and HRTEM results have confirmed that well-dispersed $MgAl_2O_4$ spinel nanoparticles are single crystals with an average particle size of 35 nm and a narrow particle size distribution.

ACKNOWLEDGMENTS

This work was supported by National Natural Science Foundation of China (11074160 and 221102087), Henan Provincial Natural Science Foundation (122102210486, 142102210481, and 142102210573), and Henan Provincial Educational Committee program (13A140824).

REFERENCES

1. O. Tokariev, L. Schnetter, T. Beck, and J. Malzbender: Grain size effect on the mechanical properties of transparent spinel ceramics. *J. Eur. Ceram. Soc.* **33**, 749–757 (2013).
2. O. Khasanov, E. Dvilis, A. Khasanov, E. Polisadova, and A. Kachaev: Optical and mechanical properties of transparent polycrystalline $MgAl_2O_4$ spinel depending on SPS conditions. *Phys. Status Solidi C* **10**, 918−920 (2013).
3. A. Rothman, S. Kalabukhov, N. Sverdlov, M. Dariel, and N. Frage: The effect of grain size on the mechanical and optical properties of spark plasma sintering-processed magnesium aluminate spinel $MgAl_2O_4$. *Int. J. Appl. Ceram. Technol.* **11**, 146–153 (2014).
4. K. Morita, B. Kim, H. Yoshida, and K. Hiraga: Spark-plasma-sintering condition optimization for producing transparent $MgAl_2O_4$ spinel polycrystal. *J. Am. Ceram. Soc.* **92**, 1208–1216 (2009).
5. S. Saha, S. Das, U.K. Ghorai, N. Mazumder, B.K. Gupta, and K.K. Chattopadhyay: Charge compensation assisted enhanced photoluminescence derived from Li-codoped $MgAl_2O_4:Eu^{3+}$ nanophosphors for solid state lighting applications. *Dalton Trans.* **42**, 12965−12974 (2013).
6. A. Ikesue and Y.L. Aung: Ceramic laser materials. *Nat. Photonics* **2**, 721–727 (2008).
7. D.W. Roy and J.L. Hastert: Polycrystalline $MgAl_2O_4$ use as windows and domes from 0.3 to 6.0 micrometer. In *1983 International Techincal Conference/Europe* (International Society for Optics and Photonics), pp. 37−43.
8. R. Cook, M. Kochis, I. Reimanis, and H.J. Kleebe: A new powder production route for transparent spinel windows: Powder synthesis and window properties. In *2005 Defense and Security* (International Society for Optics and Photonics), pp. 41–47.
9. O. Tokariev, R.W. Steinbrech, L. Schnetter, and J. Malzbender: Micro- and macro-mechanical testing of transparent $MgAl_2O_4$ spinel. *J. Mater. Sci.* **47**, 4821–4826 (2012).
10. I. Ganesh, B. Srinivas, R. Johnson, B.P. Saha, and Y.R. Mahajan: Microwave assisted solid state reaction synthesis of $MgAl_2O_4$ spinel powders. *J. Eur. Ceram. Soc.* **24**, 201–207 (2004).
11. M.M. Rashad, Z.I. Zaki, and H. EI-Shall: A novel approach for synthesis of nanocrystalline $MgAl_2O_4$ powders by co-precipitation method. *J. Mater. Sci.* **44**, 2992–2998 (2009).
12. H.J. Zhang, X.L. Jia, Z.J. Liu, and Z.Z. Li: The low temperature preparation of nanocrystalline $MgAl_2O_4$ spinel by citrate sol-gel process. *Mater. Lett.* **58**, 1625–1628 (2004).
13. G. Ye and T. Troczynski: Mechanical activation of heterogeneous sol-gel precursors for synthesis of $MgAl_2O_4$ spinel. *J. Am. Ceram. Soc.* **88**, 2970–2974 (2005).
14. A. Goldstein: Correlation between $MgAl_2O_4$-spinel structure, processing factors and functional properties of transparent parts. *J. Eur. Ceram. Soc.* **32**, 2869–2886 (2012).
15. I. Reimanis and H.J. Kleebe: A review on the sintering and microstructure development of transparent spinel ($MgAl_2O_4$). *J. Am. Ceram. Soc.* **92**, 1472–1480 (2009).
16. X. Du, S. Zhao, Y. Liu, J. Li, W. Chen, and Y. Cui: Facile synthesis of monodisperse α-alumina nanoparticles via an isolation-medium-assisted calcinations method. *Appl. Phys. A* **116**, 1963–1969 (2014).
17. M. Vu, R. Haber, and H. Gocmez: Preparation and sintering of Al_2O_3-doped magnesium aluminate spinel. In *Advances in Ceramic Armor VIII: Ceramic Engineering and Science Proceedings*, edited by J.J. Swab, M. Halbig and S. Mathur. Vol. **573**, (John Wiley & Sons, Inc., Hoboken, NJ, 2012) pp. 93–103.
18. P.Y. Lee, H. Suematsu, T. Yano, and K. Yatsui: Synthesis and characterization of nanocrystalline $MgAl_2O_4$ spinel by polymerized complex method. *J. Nanopart. Res.* **8**, 911–917 (2006).
19. M.K. Naskar and M. Chatterjee: Magnesium aluminate ($MgAl_2O_4$) spinel powders from water-based sols. *J. Am. Ceram. Soc.* **88**, 38–44 (2005).
20. M. Tahmasebpour, A.A. Babaluo, S. Shafiei, and E. Pipelzadeh: Studies on the synthesis of α-Al_2O_3 nanopowders by the polyacrylamide gel method. *Powder Technol.* **191**, 91–97 (2009).

21. G.J. Li, Z.R. Sun, C.H. Chen, X.J. Cui, and R.M. Ren: Synthesis of nanocrystalline $MgAl_2O_4$ spinel powders by a novel chemical method. *Mater. Lett.* **61**, 3585–3588 (2007).
22. R.K. Pati and P. Pramanik: Low-temperature chemical synthesis of nanocrystalline $MgAl_2O_4$ spinel powder. *J. Am. Ceram. Soc.* **83**, 1822–1824 (2000).
23. V. Montouillout, D. Massiot, A. Douy, and J.P. Couturesl: Characterization of $MgAl_2O_4$ precursor powders prepared by aqueous route. *J. Am. Ceram. Soc.* **82**, 3299–3304 (1999).
24. X. Su, X. Du, S. Li, and J. Li: Synthesis of $MgAl_2O_4$ spinel nanoparticles using a mixture of bayerite and magnesium sulfate. *J. Nanopart. Res.* **12**, 1813–1819 (2010).
25. R.M. Silverstein and F.X. Webster: *Spectrometric Identification of Organic Compounds*, 6th ed. (John Wiley & Sons, Inc., New York, 1996).
26. T. Xian, H. Yang, X. Shen, J.L. Jiang, Z.Q. Wei, and W.J. Feng: Preparation of high quality $BiFeO_3$ nanopowders via a polyacrylamide gel route. *J. Alloys Compd.* **480**, 889–892 (2009).
27. S. Kurajica, E. Tkalcec, J. Sipusic, G. Matijasic, and I. Brnardic: Synthesis and characterization of nanocrystalline zinc aluminate spinel by sol-gel technique using modified alkoxide precursor. *J. Sol-Gel Sci. Technol.* **46**, 152–160 (2008).
28. X. Du, Y. Wang, X. Su, and J. Li: Influences of pH value on the microstructure and phase transformation of aluminum hydroxide. *Powder Technol.* **192**, 40–46 (2009).
29. J.T. Kloprogge, L. Hickey, and R.L. Frost: FT-Raman and FT-IR spectroscopic study of synthetic Mg/Zn/Al-hydrotalcites. *J. Raman Spectrosc.* **35**, 967–974 (2004).
30. I.S. Park, M. Choi, T.W. Kim, and R. Ryoo: Synthesis of magnetically separable ordered mesoporous carbons using furfuryl alcohol and cobalt nitrate in a silica template. *J. Mater. Chem.* **16**, 3409–3416 (2006).
31. J.G. Li, T. Ikegami, J.H. Lee, T. Mori, and Y. Yajima: A wet-chemical process yielding reactive magnesium aluminate spinel ($MgAl_2O_4$) powder. *Ceram. Int.* **27**, 481–487 (2001).